

# Superconductivity in a single-C<sub>60</sub> transistor

Clemens B. Winkelmann<sup>\*</sup>, Nicolas Roch, Wolfgang Wernsdorfer, Vincent Bouchiat and Franck Balestro

**Single-molecule transistors are currently attracting enormous attention as possible quantum information processing devices<sup>1–5</sup>. An intrinsic limitation to their prospects, however, is associated with the presence of a small number of quantized conductance channels, each channel with a high access resistance of at best  $R_K/2 = h/2e^2 = 12.9 \text{ k}\Omega$ . However, when the contacting leads become superconducting, long-range correlations can extend throughout the whole system by means of the proximity effect. This not only lifts the resistive limitation of normal-state contacts, but further paves the way to probe electron transport through a single molecule. Here we demonstrate the realization of superconducting single-molecule transistors involving a single C<sub>60</sub> fullerene molecule. In the past few years, we have seen gate-controlled Josephson supercurrents induced in the family of low-dimensional carbon structures such as flakes of two-dimensional graphene<sup>6</sup> and portions of one-dimensional carbon nanotubes<sup>7</sup>. The present study, involving a full zero-dimensional fullerene, completes the picture.**

The rapid experimental progress in single-molecule transistors (SMTs) has revolutionized our understanding of single-spin magnetism<sup>3–5</sup>, nanoelectromechanics<sup>8,9</sup> and Kondo correlations<sup>10–12</sup>. However, no experimental realization of superconductivity in an SMT has been reported so far. Superconductivity is a central paradigm to electronic phase-coherence phenomena and its effects on SMT transport properties have been extensively investigated by theory<sup>13–15</sup>. Josephson weak links relying on bottom-up quantum-dot (QD) structures have recently been experimentally realized using semiconducting nanowires<sup>16</sup> as well as carbon nanotubes<sup>7,17,18</sup>. Superconductivity in an SMT was yet to be observed, as it offers new insights into the couplings involved in single-molecule junctions. Superconducting correlations have been observed in ungated junctions involving the metallofullerene Gd@C<sub>82</sub> (ref. 19), but the absence of supercurrents has been attributed to the destructive effect of the local magnetic moment carried by the Gd atom on the superconducting phase coherence. In this Letter, we demonstrate the first experimental realization of superconducting single-fullerene-molecular transistors, in a broad range of coupling strengths to the contacts, covering both the weakly coupled sequential tunnelling regime and the resonant tunnelling regime.

SMTs are prepared following the electromigration technique<sup>20</sup>, further optimized as presented in refs 10–12. By extending these advances to measurements at dilution refrigeration temperatures, precise electronic spectroscopies and measurements with superconducting electrodes can be undertaken. The superconducting contacts to the molecular QD are made either of aluminium, or of gold in which superconductivity is induced by the close vicinity of an aluminium capping layer (see Methods for details). After electromigration carried out at 4 K, stable devices showing

QD behaviour are further cooled and measured at 40 mK, with an effective electron temperature of 80 mK. We show here the data on four out of 11 samples that were measured at low temperature and which showed Coulomb blockade and/or gate-modulated Kondo-like features.

The superconducting weak-coupling regime is illustrated in Fig. 1b, in a device (sample A) showing two Coulomb diamonds. The conductance features of the device, which we measured for safety only up to bias voltages of  $\pm 10 \text{ mV}$ , are characteristic of single-molecular QD behaviour. The absence indeed of other conducting regions near the Fermi level over the experimentally accessible gate-voltage window ( $V_g = -4$  to  $+4 \text{ V}$ ) sets a lower bound exceeding 100 meV to the addition energy. This is large enough to rule out the possibility of an object other than a molecule, for example metallic nanoparticles<sup>21</sup>, inside the junction.

At base temperature and zero magnetic field, the conducting regions of device A do not intersect the Fermi level: they are separated by a spectroscopic source–drain voltage gap  $\Omega$  of about  $680 \mu\text{V}$  near the degeneracy point. This gap, reflecting the quasiparticle spectrum of the contacting electrodes, is a typical feature of a nanostructure weakly coupled to superconducting electrodes<sup>22</sup>. In such devices, the current is dominated by incoherent sequential tunnelling of quasiparticles of energy  $|E| > \Delta_0$  (where  $\Delta_0 = 177 \mu\text{eV}$  is the bulk superconducting gap of aluminium). The extent  $\Omega$  of the non-conducting region is very close to  $4\Delta_0/e$ , as expected in an S–I–S tunnelling structure (Fig. 1c, d). The source and drain contacts in an SMT usually have a strong geometrical asymmetry in electromigration devices (Fig. 1a). In nanostructured aluminium, superconductivity can stabilize up to much higher fields than in bulk material, exceeding 3 T in nanoscaled aluminium particles<sup>21</sup>; we may therefore expect very different critical fields in each contact. This is shown in Fig. 1c:  $\Omega$  rapidly decreases from  $4\Delta_0/e$  to about  $2\Delta_0/e$  below  $H_c = 40 \text{ mT}$ , indicative of one lead going normal, whereas superconductivity in the second lead subsists up to  $H_c \approx 0.85 \text{ T}$ , the junction being therefore of N–QD–S type at intermediate fields.

For increasing coupling to the electrodes (that is, higher conductance, assuming constant asymmetry and number of conducting channels), co-tunnelling events can occur at low bias voltage and enhance the conductance through the Kondo effect at low temperature. The increase of the QD density of states (DOS) by virtue of the Kondo effect originates from quasiparticles in the contacts lying close to the Fermi level, hopping on and off the dot. The Kondo effect and the suppression of the leads' DOS at low energies caused by superconductivity are therefore rather antagonistic processes. We illustrate the competition between Kondo correlations and superconductivity by two devices, B and C, with Kondo temperatures much larger and lower than  $T_c$  respectively. In the normal state of device B, a Coulombic addition energy  $E_{\text{add}} > 80 \text{ meV}$  is observed to coexist

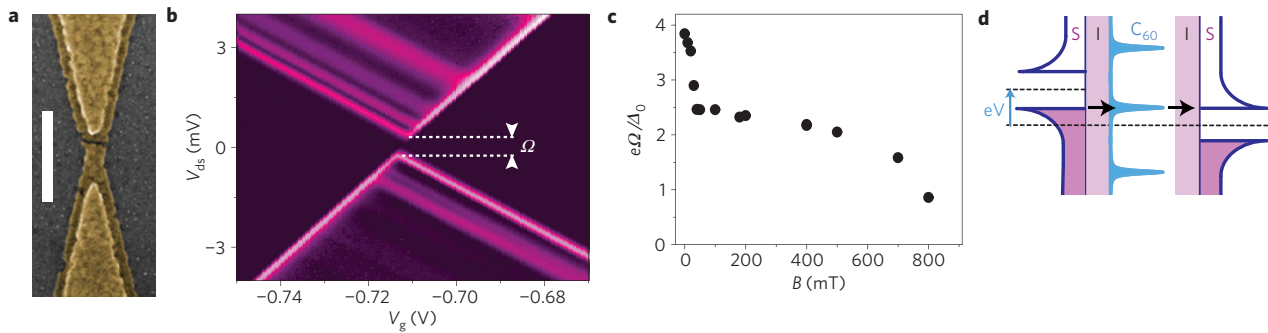


**Figure 1 | Weak-coupling limit.** **a**, SEM image of an aluminium nanogap obtained by electromigration of a constriction fabricated by angle evaporation. The scale bar is 300 nm. The nanometric gap created by the electromigration process is visible in the centre. **b**,  $\partial I/\partial V_{ds}$  differential conductance map ( $0$ – $10^{-2}e^2/h$  from dark to bright) of device A as a function of gate and bias voltage, measured at zero magnetic field and temperature  $T = 35$  mK. **c**, Extent of the non-conducting bias-voltage region at degeneracy gate voltage in sample A as a function of magnetic field. **d**, Schematic of the level alignment for minimal bias voltage conditions ( $V_{ds} = \pm 2\Delta_0/e$ ) allowing for finite current flow.

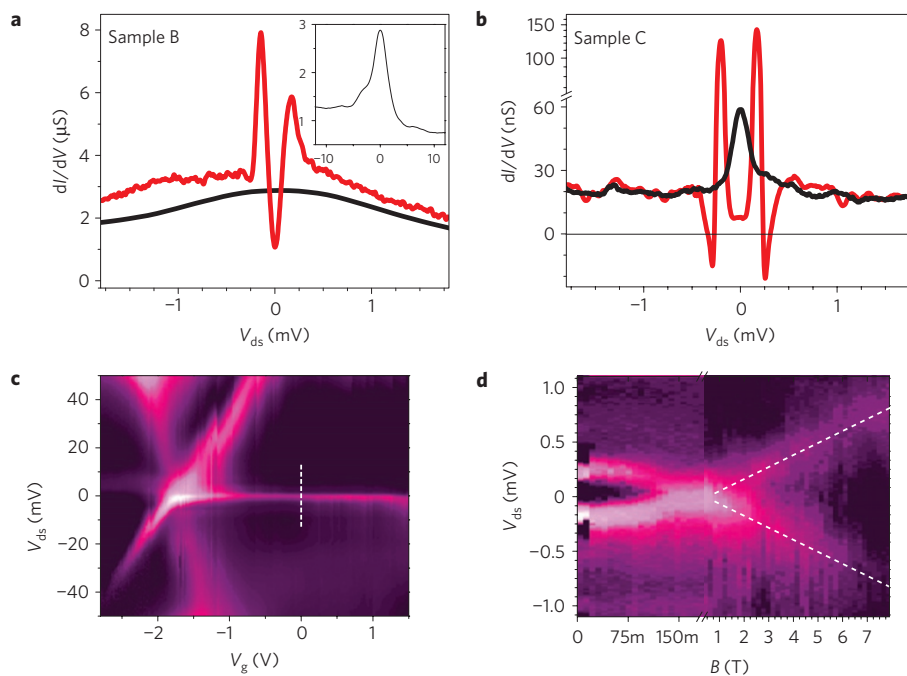


**Figure 2 | Superconductivity versus Kondo effect.** **a, b**,  $\partial I/\partial V$  as a function of drain–source voltage  $V_{ds}$  at constant gate voltage in two samples ( $T < 40$  mK) and in both the normal (black line) and the superconducting state (red line). **a**, Sample B has  $T_K = 14$  K, and superconductivity superimposes on top of the Kondo resonance. The inset shows the normal-state data over a larger bias-voltage window. **b**, Sample C has  $T_K = 0.7$  K, and the onset of superconductivity suppresses the Kondo resonance. Above 65 nS, the vertical scale is logarithmic. **c**,  $\partial I/\partial V$  map of sample B in the normal state ( $T = 40$  mK, magnetic field  $B = 400$  mT). The plots shown in **a** are taken along the dotted line (the colour code can be read from the vertical scale in **a**). **d**, Magnetic-field dependence of the low-energy  $\partial I/\partial V$  in sample C. At about 130 mT, the coherence peaks merge into the Kondo resonance, which is further Zeeman split above  $B_c \approx 0.4$  T. The dotted lines are fits to the Zeeman splitting (see text). For better contrast, the  $\partial I/\partial V$  colour code is different in the low- and high-field regions.

with rather strong lead coupling, translating into a large Kondo resonance with Kondo temperature  $T_K = 14$  K (Fig. 2c, details in the Supplementary Information). In the superconducting state of the leads, superconductivity does not suppress the Kondo resonance and the superconducting features such as the coherence peaks at  $V_{ds} = \pm 2\Delta_0/e$  superimpose on top of it (Fig. 2a). Such a behaviour was predicted<sup>13,23</sup> and previously observed<sup>24,25</sup> in other types of QD device verifying  $T_K \gg T_c$ . The opposite limit  $T_K < T_c$  is illustrated by the more weakly coupled device C (Fig. 2c), which similarly showed a Coulomb blockade and Kondo resonance pattern, but with a much lower  $T_K = 0.7$  K. In the superconducting state, the Kondo peak at the Fermi level is destroyed<sup>13,24</sup>. Interestingly, inside this Coulomb diamond, corresponding to an odd occupation

number, that is, to a local magnetic moment no longer screened by the lead electrons, the differential conductance is not maximum at  $V_{ds} = \pm 2\Delta/e$ . Further, a sign inversion of the differential conductance is observed, which is most prominent close to the degeneracy points. This negative differential conductance, as already reported in larger superconducting QD systems<sup>22,26,27</sup>, results from Fermi's golden rule applied to the superconducting leads' DOSs, which are convoluted with the delta-function-like DOS of the QD. The gradual reduction of the superconducting gap under applied magnetic field re-establishes the Kondo resonance (Fig. 2d). For magnetic fields  $B > B_c \approx 400$  mT the resonance is Zeeman split, with a splitting energy  $E_Z = \pm g \Delta S \mu_B (B - B_c)$ . Here,  $g$  is the electron Landé factor,  $\Delta S$  the difference between the two

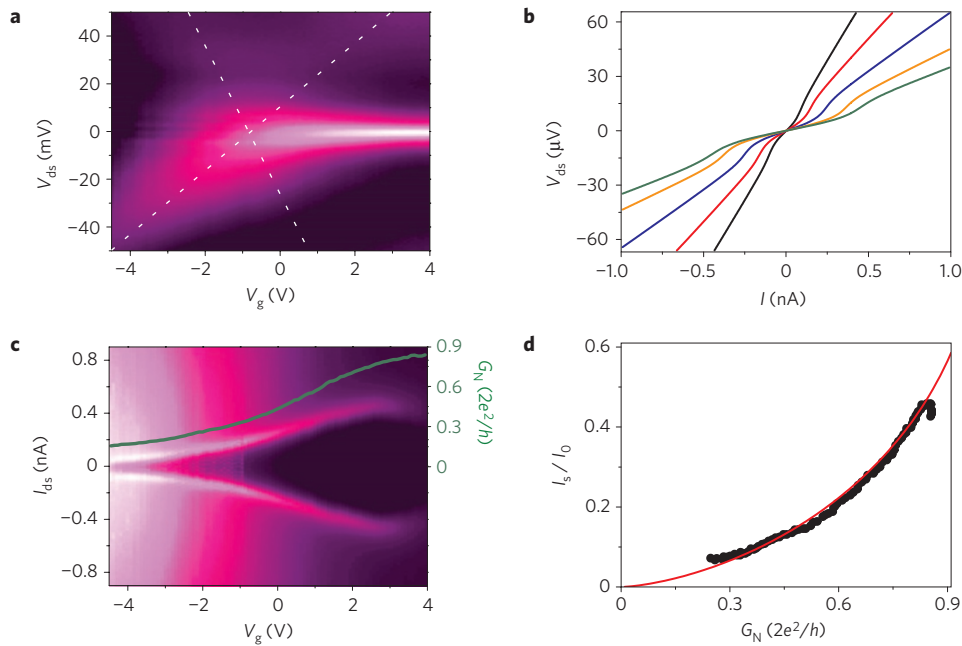


**Figure 3 | Gated Josephson supercurrent in a single C<sub>60</sub>.** **a**,  $\partial I/\partial V$  map (0–1.7 $e^2/h$  from dark to bright) of device D as a function of gate and bias voltage in the normal state ( $B = 20$  mT). The dotted lines emphasize the Coulomb diamond edges. **b**, Drain-source voltage  $V_{ds}(I)$  in the superconducting state for  $V_g = -3, -1.5, 0, 1.5, 3$  V from black to green. **c**, Differential resistance map (7–110 k $\Omega$  from dark to bright) in the superconducting state ( $B = 0$  T) for small bias currents modulated by  $I_{mod} = 18$  pA at  $f_0 = 86$  Hz. The green line is the linear conductance in the normal state. **d**, Switching current  $I_s$  normalized to  $I_0 = 1.01$  nA as a function of normal-state conductance (bullets), and fitted to equation (1) (line). The only adjustable parameter is  $I_0$ . The data points deviating from the fit at high conductance correspond to measurements made at  $V_g \approx 4$  V, where a significant tunnel leakage current from the gate electrode contaminated the measurements.

spin states and  $\mu_B$  the Bohr magneton. As  $\Delta S = 1$ , we find here  $g = 1.84 \pm 0.2$  along the best linear fit, given by the dotted lines.

Moving on to high coupling strengths  $T$ , we show that Josephson supercurrent can be observed in SMTs. In equilibrium, dissipationless transport across an S–QD–S structure is achieved by co-tunnelling of Cooper pairs. The Josephson current amplitude  $I_c$  therefore scales with  $T^2$  and is experimentally accessible only for relatively strong coupling to the leads. Device D illustrates the molecular-junction behaviour in this regime. In the normal state (Fig. 3a), the differential conductance map shows a zero-bias resonance for positive gate voltages on a ridge delimited by only faintly visible Coulomb diamond edges. In this regime the electrostatic on-site repulsion is largely overcome by the strong coupling to the leads. The maximum differential conductance  $G_N \sim 0.85 \times (2e^2/h)$  observed here approaches the unitary limit. If analysed in terms of a Kondo resonance, the width of the resonance yields a large  $T_K \approx 80$  K, as already reported in normal SMTs in the past<sup>28</sup>. In voltage-biased measurements of the superconducting state, the differential conductance around the Fermi level shows the usual coherence peaks at  $V_{ds} = \pm 2\Delta/e$  with  $\Delta \approx 120$   $\mu$ eV (not shown, similar to Fig. 2a). For supercurrent measurements, however, a current bias is better adapted. Figure 3b shows  $V_{ds}(I)$  measurements for different gate voltages, showing the gate dependence of the critical current. In more detail, Fig. 3c shows a  $\partial V/\partial I$  differential resistance map for small bias currents. The ridge visible here defines a switching current  $I_s$  such that  $\partial^2 V/\partial I^2|_{I_s} = 0$ . For  $|I| < I_s$  the differential resistance is strongly reduced below  $R_j$ . The quality factor of the junction is  $Q \approx 1$  (see Supplementary Information), and the absence of hysteresis observed here indicates that fluctuations are damped out. The residual resistance below  $I_s$  is related to the phase diffusion of the Josephson state along the ‘tilted washboard’ potential<sup>29</sup>. Such features are generic to small Josephson junctions with a large normal-state resistance, even for quality factors larger than unity<sup>29</sup>. Another feature common

to small Josephson junctions is the strong reduction of the switching current with respect to the ideal critical current value  $I_0(R_j) = \Delta/eR_j$  (equal to 6–20 nA here, depending on the gate voltage), and is understood as an effect of finite temperature and environmental coupling (for example, to phonons on the quantum dot<sup>14</sup> or electromagnetic modes in the leads). In an unshunted junction hosting a single spin-degenerate conductance channel, the coupling to the environmental admittance is expected<sup>7,30</sup> to produce a reduction of the switching current following

$$I_s/I_0 = (1 - \sqrt{1 - G_N h/2e^2})^{3/2} \quad (1)$$

Experimentally, this 3/2 power-law dependence was observed to hold in metallic superconducting single-electron transistors<sup>30</sup> and in carbon-nanotube junctions<sup>7</sup>. The fit of the  $I_s(G_N)$  data shown in Fig. 3d to equation (1) yields  $I_0 = 1.01$  nA. It is remarkable that, whereas the justification of equation (1) strictly holds for weakly damped junctions<sup>30</sup>, a very good agreement with experiment is still found in device D, which is at the crossover between the two damping regimes.

This experiment demonstrates the coexistence and competition of the effects of Coulomb repulsion, Kondo correlations and superconductivity in C<sub>60</sub> SMTs over a broad range of lead coupling strengths. In contrast with previous experiments involving carbon-nanotube junctions<sup>7</sup> the energy spectrum is fixed here by the molecular edifice itself and not by the nanoengineered portion of nanotube linking the contacting electrode. This experiment paves the way for further studies targeting phase-sensitive measurements and the interplay of superconductivity with magnetically active molecules such as endofullerenes<sup>5,19</sup>. Future efforts may point to molecular Q-bit architectures by integrating a gated magnetic molecule Josephson weak link into a SQUID geometry.

## Methods

The starting material for the devices is thin metallic wires with a local constriction about 100 nm wide and 20 nm thick, defined by e-beam lithography and double-angle evaporation through a suspended mask, on top of a local Al/Al<sub>2</sub>O<sub>3</sub> backgate (Fig. 1a), as described in ref. 12. C<sub>60</sub> diluted in toluene is drop-cast on the thoroughly cleaned devices, which are then immediately introduced into the sample mount thermally anchored to the mixing chamber of a dilution refrigerator. The electronic base temperature of the set-up was determined in an independent experiment, in which we measured transport across planar N–I–S junctions (Cu/Al<sub>2</sub>O<sub>3</sub>/Al). The Bardeen–Cooper–Schrieffer fit to the data yielded an upper bound of 80 mK.

At liquid-helium temperatures, the bias voltage across the wires is ramped up until the electromigration process sets on. The device resistance, which has an initial value of about 100 Ω, increases, often stepwise, indicating the breaking up of individual one-dimensional atomic conduction channels. As soon as the device resistance exceeds 12.9 kΩ, the bias voltage is cancelled within microseconds. After electromigration, the junctions are further cooled down to sub-0.1 K temperatures. About 50% of all electromigrated junctions show a tunnelling transport behaviour with a low bias resistance  $R_K < R_j < 1$  GΩ. About 10% of these further show a gate-dependent signal, indicative of QD behaviour. High bandwidth control of the electromigration process is known to strongly increase the yield for obtaining narrow tunnelling junctions. Two types of superconducting electromigration junction have been investigated: all aluminium electromigration junctions and proximity superconducting Al/Au junctions. In the latter, the tunnel junction is opened through a short ( $L < 150$  nm) and thin gold wire connected to nearby larger superconducting aluminium source and drain pads (for details see Supplementary Information).

The method used here for nanogap formation requires a low-impedance environment to keep the bandwidth during electromigration high enough during conductance monitoring. This forbids the implementation of chip resistors, thereby preventing a full control of the electromagnetic environment. We measured 11 samples that showed stable and non-pathological gate-dependent conductance features. Four of them were weakly coupled, showing Coulomb blockade but no Kondo resonance. Two other devices showed a weak Kondo resonance ( $T_K < T_c$ ), whereas the remaining five were in the opposite limit. Device D showed the largest  $T_K$  and was the only junction to have a critical current approaching the nA range.

Received 20 April 2009; accepted 15 September 2009;  
published online 25 October 2009

## References

- Leuenberger, M. N. & Loss, D. Quantum computing in molecular magnets. *Nature* **410**, 789–793 (2001).
- Romeike, C., Wegewijs, M. R. & Schoeller, H. Spin quantum tunneling in single molecular magnets: Fingerprints in transport spectroscopy of current and noise. *Phys. Rev. Lett.* **96**, 196805 (2006).
- Heersche, H. B. *et al.* Electron transport through single Mn12 molecular magnets. *Phys. Rev. Lett.* **96**, 206801 (2006).
- Jo, M. H. *et al.* Signatures of molecular magnetism in single-molecule transport spectroscopy. *Nano Lett.* **6**, 2014–2020 (2005).
- Grose, J. E. *et al.* Tunneling spectra of individual magnetic endofullerene molecules. *Nature Mater.* **7**, 884–889 (2008).
- Heersche, H. B., Jarillo-Herrero, P., Oostinga, J. B., Vandersypen, L. M. K. & Morpurgo, A. F. Bipolar supercurrent in graphene. *Nature* **446**, 56–59 (2007).
- Jarillo-Herrero, P., van Dam, J. A. & Kouwenhoven, L. P. Quantum supercurrent transistors in carbon nanotubes. *Nature* **439**, 953–956 (2006).
- Park, H. *et al.* Nanomechanical oscillations in a single-C60 transistor. *Nature* **407**, 57–60 (2000).
- Pasupathy, A. N. *et al.* Vibration-assisted electron tunneling in C140 transistors. *Nano Lett.* **5**, 203–207 (2005).
- Park, J. *et al.* Coulomb blockade and the Kondo effect in single-atom transistors. *Nature* **417**, 722–725 (2002).
- Liang, J. *et al.* Kondo resonance in a single-molecule transistor. *Nature* **417**, 725–729 (2002).
- Roch, N., Florens, S., Bouchiat, V., Wernsdorfer, W. & Balestro, F. Quantum phase transition in a single-molecule quantum dot. *Nature* **453**, 633–638 (2008).

- Choi, M.-S., Lee, M., Kang, K. & Belzig, W. Kondo effect and Josephson current through a quantum dot between two superconductors. *Phys. Rev. B* **70**, 020502(R) (2004).
- Novotný, T., Rossini, A. & Flensberg, K. Josephson current through a molecular transistor in a dissipative environment. *Phys. Rev. B* **70**, 224502 (2005).
- Lee, M., Jonckheere, T. & Martin, T. Josephson effect through a magnetic metallofullerene molecule. *Phys. Rev. Lett.* **101**, 146804 (2008).
- Doh, Y.-J. *et al.* Tunable supercurrent through semiconductor nanowires. *Science* **309**, 272–275 (2005).
- Cleuziou, J. P., Wernsdorfer, W., Bouchiat, V., Ondarcuhu, T. & Monthieux, M. Carbon nanotube superconducting quantum interference device. *Nature Nanotech.* **1**, 53–59 (2006).
- Jørgensen, H. I., Grove-Rasmussen, K., Novotný, T., Flensberg, K. & Lindelof, P. E. Electron transport in single-wall carbon nanotube weak links in the Fabry–Perot regime. *Phys. Rev. Lett.* **96**, 207003 (2006).
- Kasumov, A. K. *et al.* Proximity effect in a superconductor–metallofullerene–superconductor molecular junction. *Phys. Rev. B* **72**, 033414 (2005).
- Park, H., Lim, A. K. L., Park, J., Alivisatos, A. P. & McEuen, P. L. Fabrication of metallic electrodes with nanometre separation by electromigration. *Appl. Phys. Lett.* **75**, 301–303 (1999).
- Black, C. T., Ralph, D. C. & Tinkham, M. Spectroscopy of the superconducting gap in individual nanometre-scale aluminum particles. *Phys. Rev. Lett.* **76**, 688–691 (1996).
- Ralph, D. C., Black, C. T. & Tinkham, M. Spectroscopic measurement of discrete electronic states in single metal particles. *Phys. Rev. Lett.* **74**, 3241–3244 (1995).
- Glazman, L. I. & Matveev, K. A. Resonant Josephson current through Kondo impurities in a tunnel barrier. *Pisma Zh. Tekh. Fiz.* **49**, 570–573 (1988); *JETP Lett.* **49**, 659–662 (1989).
- Buitelaar, M. R., Nussbaumer, T. & Schönberger, C. Quantum dot in the Kondo regime coupled to superconductors. *Phys. Rev. Lett.* **89**, 256801 (2002).
- Buizert, C., Oiwa, A., Shibata, K., Hirakawa, K. & Tarucha, S. Kondo universal scaling for a quantum dot coupled to superconducting leads. *Phys. Rev. Lett.* **99**, 136806 (2007).
- Eichler, A. *et al.* Even–odd effect in Andreev transport through a carbon nanotube quantum dot. *Phys. Rev. Lett.* **99**, 026601 (2007).
- Doh, Y.-J., De Franceschi, S., Bakkers, E. P. A. M. & Kouwenhoven, L. P. Andreev reflection versus Coulomb blockade in hybrid semiconductor nanowire devices. *Nano Lett.* **8**, 4098–4102 (2008).
- Yu, L. H. & Natelson, D. The Kondo effect in C<sub>60</sub> single-molecule transistors. *Nano Lett.* **4**, 79–83 (2004).
- Tinkham, M. *Introduction to Superconductivity* 2nd edn (McGraw-Hill, 1995).
- Joyez, P., Lafarge, P., Filipe, A., Esteve, D. & Devoret, M. H. Observation of parity-induced suppression of Josephson tunnelling in the superconducting single electron transistor. *Phys. Rev. Lett.* **72**, 2458–2461 (1994).

## Acknowledgements

This project was funded by the French ANR-PNANO contract Molspintronics. We would like to thank E. Eyraud, D. Lepoittevin, Th. Fournier and Th. Crozes for technical assistance and T. Martin, M. Lee, Th. Jonckheere, D. Feinberg and H. Courtois for discussions. The samples were fabricated in the Nanofab facilities at the Institut Néel.

## Author contributions

C.B.W. made the superconducting electromigration devices and carried out the experiment. N.R. developed the sample fabrication and measurement techniques involved, with the help of F.B. C.B.W., V.B. and F.B. wrote the manuscript, with the help of all other authors. V.B., W.W. and F.B. conceived the experiment and directed the research.

## Additional information

Supplementary information accompanies this paper on [www.nature.com/naturephysics](http://www.nature.com/naturephysics). Reprints and permissions information is available online at <http://npg.nature.com/reprintsandpermissions>. Correspondence and requests for materials should be addressed to C.B.W.